A. F. Garcia-Fernandez, J. Grajal and O. A. Yeste-Ojeda, "Back-Scattering of a Helicopter with a Millimeter-Wave LFMCW Radar," in IEEE Transactions on Aerospace and Electronic Systems, vol. 49, no. 4, pp. 2781-2792, OCTOBER 2013, doi: 10.1109/TAES.2013.6621853.

Back-scattering of a helicopter with a millimeter-wave LFMCW Radar

Ángel F. García-Fernández, Jesús Grajal, Omar A. Yeste-Ojeda

Abstract

This paper proposes a simulator to obtain the radar back-scattering of a helicopter. Due to the high rotational speed of the blades, their tips move several wavelength during the transmitted ramp and the stop-and-go assumption is not valid anymore. The results of the simulator are supported by experimental data.

Index Terms

Facet model, helicopter, LFMCW, modelling, radar backscattering, millimeter-wave radar

I. Introduction

An increasingly demanded application during peace keeping missions under war conditions is non-cooperative target classification of vehicles, where the unexpected appearance of friendly or threatening vehicles must be considered. A typical example is a helicopter armed or equipped for humanitarian tasks [1]. Consequently, helicopter classification is a very important matter. To perform the classification, inverse synthetic aperture radar (ISAR) images [1]–[5] and returned echoes [6]–[10] can be used.

It is very complicated to carry out controlled experiments to measure the back-scattered signal from a target, so the development of a simulator is of great help to extract its main features and develop classification algorithms. The simulator must generate data for realistic waveforms, with accurate scattering models and realistic targets' dynamics and, we cannot overlook that its output should be validated

The authors are with the Grupo de Microondas y Radar, Departamento de Señales, Sistemas y Radiocomunicaciones, ETSI de Telecomunicación, Universidad Politécnica de Madrid, Ciudad Universitaria s/n, 28040 Madrid, Spain. emails:{agarcia, jesus, omar}@gmr.ssr.upm.es.

This work was supported in part by the Spanish national research and development program under Project TEC2011-28683-C02-01. The authors thank A. Blanco-del-Campo, A. Asensio-López and B. P. Dorta-Naranjo for providing us with the measured data of the helicopter and J. M. Muñoz-Ferreras for compensating the motion of the measured data.

by measurements. When a linear frequency modulated continuous wave (LFMCW) radar is used, the returned echoes are usually simulated under the stop-and-go assumption. This refers to the fact that the scatterers that make up the target are assumed to be stationary during the pulse ramp. However, if the target has any fast moving or rotating parts, such as the blades of a helicopter or the propellers of an aircraft, the returns generated by these structures cannot be modelled by the stop-and-go assumption since some scatterers move some wavelengths during the typical LFMCW ramp duration. This results in the expansion of the power of the signal along the range axis [11], [12].

The novelties introduced by this paper are twofold. First, we use a mathematical model to study the radar back-scattering signal of a helicopter blade. This study generalises the one in [11] as it considers elevation angles different to zero and the accelerations of the scatterers. This mathematical model does not take into account the radar cross section of the blades nor the shadowing. Second, a computationally-efficient simulator is proposed to take into account the radar cross section and shadowing effects without requiring the stop-and-go assumption. The scattering model in our simulation tool is based on perfectly conducting triangular facets [13]–[15]. This model has two advantages. It requires much less computational burden than the electromagnetic model [16] and provides much more realistic images than the point-scatterer model [17], [18]. Importantly, the simulator results are supported by measured data captured with the LFMCW radar described in [19].

The rest of the paper is organised as follows. In Section II, we generalise the results obtained in [11] developing a mathematical model to study the radar back-scattering signal of a helicopter blade varying its elevation angle but without radar cross section considerations. In Section III, we adapt the facet model proposed in [13], [14] so that the simulator does not work under the stop-and-go assumption. We analyse the results provided by our simulator in Section IV. The results of our simulator are supported by measured data in Section V. Finally, conclusions are drawn in Section VI.

II. Theoretical approach to blade echo modelling

The purpose of this section is not to provide an accurate model of the echo of a helicopter blade, which will be given in Section III, but to provide a simple model with several aims. First, it demonstrates that the stop-and go assumption is no longer valid to model helicopter blades for different elevation angles. Second, it demonstrates that assuming that the accelerations of the scatterers are zero is reasonable for the usual parameters of helicopter blades. Third, it shows that the received signal from a helicopter blade expands in the range axis for different elevation angles.

The assumptions made in this paper are:

- Assumption 0 (stop-and-go): the scatterers remain in the same position during the LFMCW ramp duration.
- Assumption 1: the scatterers have a constant linear velocity during the LFMCW ramp duration.
- Assumption 2: the scatterers have a constant linear acceleration during the LFMCW ramp duration.

It should be noted that Assumption i indicates that the movement of the scatterers during the LFMCW ramp duration is modelled as an ith order polynomial. Therefore, Assumption 0 is more restrictive than Assumption 1 and Assumption 1 is more restrictive than Assumption 2.

The aims of this section are attained by showing the effect of Assumptions 0-2 on the range profiles for an LFMCW radar with a stationary antenna. We do not take into account the different radar cross sections of the scatterers that make up the blade. This will be done in Section III using a simulator based on facets [13].

A. LFMCW returned signal from one scatterer

For an LFMCW radar, the transmitted signal is [20]

$$s\left(t\right)=e^{j(2\pi f_{c}t+\pi\gamma t^{2})} \tag{1}$$

where γ is the chirp rate, f_c is the central frequency, $t\in[-T_{ramp}/2,\,T_{ramp}/2]$ and T_{ramp} is the LFMCW ramp duration.

The received signal $r\left(t\right)$ has a time dependent delay $\tau\left(t\right)$ with respect to the transmitted signal that must satisfy [21]

$$\tau\left(t\right)=\frac{2}{c}R\left(t-\frac{\tau\left(t\right)}{2}\right) \tag{2}$$

where c is the speed of light. Therefore,

$$r\left(t\right)=s\left(t-\tau\left(t\right)\right) \tag{3}$$

where we have not taken into account the attenuation of the signal. The returned signal after the process of dechirping from a scatterer illuminated with an LFMCW radar is [20]:

$$s_{r}\left(t\right)=s\left(t\right)r^{\star}\left(t\right) \tag{4}$$

where $r^{\star}\left(t\right)$ is the conjugate of $r\left(t\right)$. In the following, we provide the expression of (4) under Assumptions 0, 1 and 2.

1) Derivation under Assumption 0: Under Assumption 0, the range $R(t)$ of a scatterer during the ramp duration is

$$R\left(t\right) = R_0 \tag{5}$$

where R_0 is the range of the scatterer at the beginning of the ramp.

Substituting (5) into (2), the delay is

$$\tau\left(t\right) = \frac{2}{c} R_0 \tag{6}$$

and the returned signal after the process of dechirping, see (4), can be written as [20]

$$s_0(t) = e^{j(\phi_{10} + \phi_{11} t)} \tag{7}$$

where

$$\phi_{10} = \frac{4\pi f_c R_0}{c} - \frac{4\pi\gamma R_0^2}{c^2} \tag{8}$$

$$\phi_{11} = \frac{4\pi\gamma R_0}{c} \tag{9}$$

2) Derivation under Assumption 1: Under Assumption 1, the range $R(t)$ of a scatterer during the ramp duration is

$$R(t) = R_0 + v_R t \tag{10}$$

where v_R is the radial velocity of the scatterer and R_0 is the range of the scatterer at the beginning of the ramp.

Substituting (10) into (2), the delay is

$$\tau\left(t\right) = \frac{2}{c + v_R} \cdot \left(R_0 + v_R t\right) \tag{11}$$

Taking into account this time dependent delay, for $t \in [-T_{ramp}/2,\, T_{ramp}/2]$, the returned signal after the process of dechirping, see (4), is [11]

$$s_1(t) = e^{j(\phi_{20} + \phi_{21} t + \phi_{22} t^2)} \tag{12}$$

where

$$\phi_{20} = \frac{4\pi f_c R_0}{c + v_R} - \frac{4\pi\gamma R_0^2}{\left(c + v_R\right)^2} \tag{13}$$

$$\phi_{21} = \frac{4\pi f_c v_R}{c + v_R} + \frac{4\pi\gamma R_0 \left(c - v_R\right)}{\left(c + v_R\right)^2} \tag{14}$$

$$\phi_{22} = \frac{4\pi\gamma v_R c}{\left(c + v_R\right)^2} \tag{15}$$

It should be noticed that (7) can be obtained from (12) setting the scatterer radial velocity to zero, $v_R = 0$.

3) Derivation under Assumption 2: Under Assumption 2, the range $R(t)$ of a scatterer during the ramp duration is

$$R(t) = R_0 + v_R t + \frac{1}{2} a_R t^2 \tag{16}$$

where a_R is the radial acceleration of the scatterer at the beginning of the ramp.

Substituting (16) into (2), we get

$$\frac{a_R}{4c}\tau^2(t) - \left(\frac{v_R + a_R t}{c} + 1\right)\tau(t) + \frac{2}{c}\left(R_0 + v_R t + \frac{1}{2} a_R t^2\right) = 0 \tag{17}$$

Equation (17) has two solutions for $\tau(t)$ but there is only one, which is denoted as $\tau_1(t)$, that makes sense, i.e., it is in a reasonable range of time delays. We want to remark that we do not provide the straightforward analytical expression for the solutions of (17) because they are numerically unstable for the typical values of radial velocity and acceleration of a helicopter blade, see Section II-B. We found the solutions calculating the eigenvalues of the companion matrix[1] [22].

Using (4), the returned signal after the process of dechirping is

$$s_2(t) = s(t)\, s^\star(t - \tau_1(t)) \tag{18}$$

B. LFMCW returned signal from a helicopter blade

In this section, we study the effect of varying the elevation angle of a blade on the range profiles without radar cross section considerations. The geometry of the analysis is shown in Figure 1. The blade is moving with an angular velocity Ω with respect to one of its ends, which is stationary. The blade has a length L, the radar is located at the origin of the coordinate system $OUVW$, the distance from the radar to the rotation center of the blade is R_c, the blade rotates in a plane parallel to OUV and the rotation center of the blade is located on the OUW plane with an elevation angle of α. Although this is a particular case in which the plane of movement of the blade is parallel to the OUW plane, it can be generalised just by changing the definition of the coordinate system $OUVW$. In this case, it would depend on the plane of movement of the blade, see the appendix for details.

As an LFMCW waveform is used, the range profiles are obtained by applying a fast Fourier transform (FFT) to the received signal after dechirping during each ramp. The range profiles are similar to the spectrogram of the received signal if we use a short time Fourier transform (STFT) with a window that lasts T_{ramp} and without overlapping of the FFTs.

[1]This algorithm is implemented in Matlab in the function "roots".

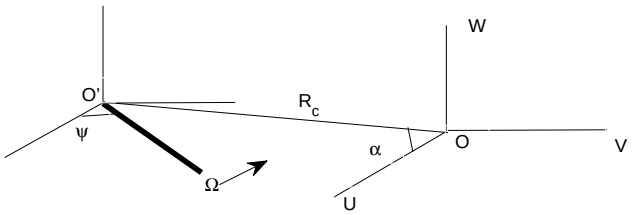

Figure 1: Geometry of the blade echo analysis. The blade, which is represented with a thicker line, is rotating with an angular velocity Ω and an arrow indicates its direction of rotation. The radar is located at O. The blade is orthogonal to the line of sight for $\psi = 90$º.

The received signal from the blade $b_i(t)$, assuming that the whole blade is composed of infinitesimal identical scatterers, under Assumption i is:

$$b_i(t) = \int_0^L b_{s,i}(t, l)\, dl \tag{19}$$

where the integral is performed along the dimension of the blade l and $b_{s,i}(t, l)$ is the returned signal from an infinitesimal scatterer located at a distance l along the blade from the blade rotation axis under Assumption i. Therefore, $b_{s,i}(t, l)$ is equal to $s_i(t)$, which is given by (7), (12) and (18), but substituting R_0, v_R and a_R by $R_0(l)$, $v_R(l)$ and $a_R(l)$ to highlight that the range, the radial velocity and radial acceleration depend on the distance from the rotation axis of blade to the point under consideration.

Now, we proceed to the calculation of $R_0(l)$, $v_R(l)$ and $a_R(l)$ when the blade forms an angle of ψ with the $O'U$ axis at the beginning of the ramp. The vector that goes from the rotation axis of the blade to a point P that is located at a distance l along the blade is

$$\overrightarrow{O'P} = (l\cos\psi,\, l\sin\psi,\, 0) \tag{20}$$

The vector that goes from the radar to the stationary end of the blade is

$$\overrightarrow{OO'} = (R_c\cos\alpha,\, 0,\, R_c\sin\alpha) \tag{21}$$

Therefore, the vector that goes from the radar to P is

$$\overrightarrow{OP} = \overrightarrow{OO'} + \overrightarrow{O'P} = (l\cos\psi + R_c\cos\alpha,\, l\sin\psi,\, R_c\sin\alpha) \tag{22}$$

Then, $R_0(l)$ is obtained by calculating the norm of the vector $\overrightarrow{OP}$, equation (22)

$$R_0(l) = \left|\overrightarrow{OP}\right| = \sqrt{l^2 + R_c^2 + 2lR_c\cos\psi\cos\alpha} \tag{23}$$

Applying the change of variable $a = l/R_c$, equation (23) becomes

$$R_0(a) = R_c \cdot \sqrt{a^2 + 1 + 2a\cos\psi\cos\alpha} \tag{24}$$

Assuming that $R_c \gg l$, i. e., $a \ll 1$, and applying a linear approximation to equation (24)

$$R_0(a) \approx R_0(0) + a \cdot \frac{dR_0(0)}{da} \tag{25}$$

Calculating the derivative and changing back to the variable $l = a \cdot R_c$ in equation (25)

$$R_0(l) \approx R_c + l\cos\psi\cos\alpha \tag{26}$$

The velocity vector $\overrightarrow{v(l)}$ can be calculated as

$$\overrightarrow{v(l)} = \overrightarrow{\Omega} \times \overrightarrow{O'P} \tag{27}$$

where $\overrightarrow{\Omega} = (0,\, 0,\, \Omega)$ is the angular velocity vector. Then, substituting (20) in (27), we get

$$\overrightarrow{v(l)} = (-\Omega l\sin\psi,\, \Omega l\cos\psi,\, 0) \tag{28}$$

The radial velocity (with respect to the radar) is calculated as

$$v_R(l) = \overrightarrow{v(l)} \cdot \frac{\overrightarrow{OP}}{R_0(l)} \tag{29}$$

Substituting (22), (26) and (28) in (29)

$$v_R(l) = \frac{-R_c\Omega l\cos\alpha\sin\psi}{R_c + l\cos\psi\cos\alpha} \tag{30}$$

The acceleration vector $\overrightarrow{a(l)}$ can be calculated as

$$\overrightarrow{a(l)} = \overrightarrow{\Omega} \times \overrightarrow{v(l)} \tag{31}$$

$$= \left(-\Omega^2 l\cos\psi, -\Omega^2 l\sin\psi, 0\right) \tag{32}$$

The radial acceleration is

$$a_R(l) = \overrightarrow{a(l)} \cdot \frac{\overrightarrow{OP}}{R_0(l)} \tag{33}$$

Substituting (22), (26) and (32) in (33):

$$a_R(l) = -\Omega^2 l\left(\frac{l + R_c\cos\psi\cos\alpha}{R_c + l\cos\psi\cos\alpha}\right) \tag{34}$$

Now, we obtain the range profiles for two elevation angles α =0º and α =80º, several values of ψ and the simulation parameters, which are typical values for helicopter blades, shown in Table[2] I. As indicated

[2]Note that the sampling frequency can be much lower than the transmitted bandwidth as we know where we are placing the blade. This saves a lot of computational power. See [14, Sec. III] for more details.

Table I: Parameters of blade simulation

Parameter	Value
Central frequency f_c	28.5 GHz
Bandwidth B	200 MHz
PRF	1 kHz
T_{ramp}	0.9 ms
Chirp rate γ	$2.22 \cdot 10^{11}$ Hz/s
Sampling frequency	2 MHz
FFT window	Hamming
R_c	1000 m
Angular velocity Ω	43 rad/s
Blade length L	5 m

before, the range profiles are calculated by applying an FFT to each ramp of the received signal, equation (19). In the simulations, we also use a Hamming window to reduce the side-lobes when we calculate the FFT. Then, as it is an LFMCW radar, there is a correspondence between the beat frequency f_b after the process of dechirping and the distance R of the scatterer that produces that frequency [20]

$$R = \frac{c \cdot f_b \cdot T_{ramp}}{2 \cdot B} \tag{35}$$

Taking equation (35) into account, we show the range profiles for elevation angle α =0º in Figure 2. There are very important differences between the figures under Assumptions 1 and 2 and the figure under Assumption 0. Under Assumptions 1 and 2, there is an expansion of the power of the signal along the range axis that does not happen under Assumption 0 (stop-and-go). Therefore, the stop-and-go assumption is not appropriate to model the received signal from the blades. This expansion is powerful and flat when the blade is orthogonal to the line of sight, $\psi = 90$º, and its length decreases as the angle of elevation rises. When the blade is not orthogonal to the line of sight, the expansion of the power of the signal is not flat anymore and there are two peaks. These two peaks appear on account of the fact that, in this case, there are constructive and destructive interference phenomena along the blade [11]. Figures 2(a) and 2(b) are quite similar although there are some differences. For $\psi = 90$º and $\psi = 85$º, the figures are alike but for $\psi = 45$º and $\psi = 0$º there are some subtle differences. For both cases, the width of the peak that is not located at 1000 m is slightly wider under Assumption 2. Nevertheless, the difference is very slight.

In Figure 3, we show the range profiles for elevation angle α =80º. In this case, the difference between

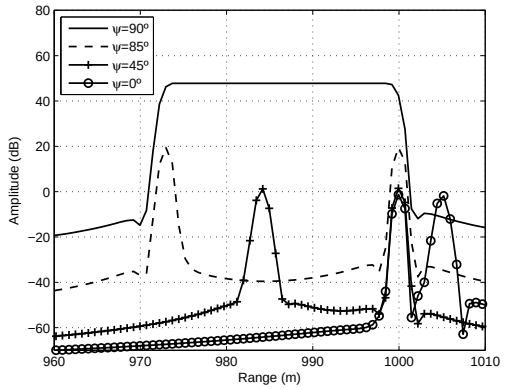

(a)

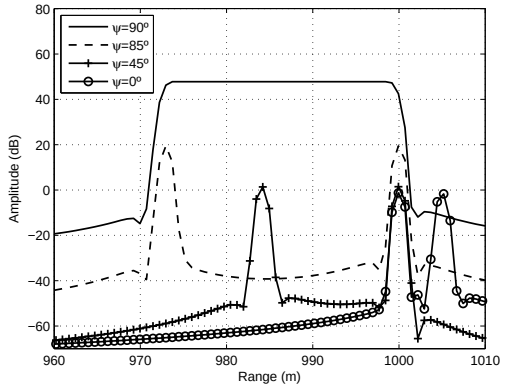

(b)

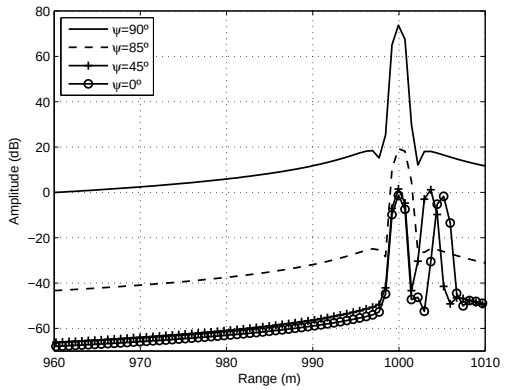

(c)

Figure 2: Range profiles of a single blade using the theoretical model in Section II for an angle of elevation α =0º: (a) Under Assumptions 2 (b) Under Assumption 1 (c) Under Assumption 0 (stop-and-go). The stop-and-go assumption is not valid for simulating the radar back-scattering from a helicopter blade using an LFMCW radar. Assumptions 1 and 2 produce quite similar results.

the figures under Assumptions 1 and 2 and the figure under Assumption 0 is also significant but less than for $\alpha = 0^{\circ}$. However, in this case, the figures under Assumption 1 and 2 are alike. This supports the fact that Assumption 1 is reasonable enough to model helicopter blades in our simulator, which is described in Section III.

Real helicopters have more than one blade and, consequently, there is an interaction between the blades due to the shadowing and the contribution of several blades to the received signal. Then, even though this theoretical study provides a lot of insight into this problem, it is not an accurate modelling of the problem because it does not take into account the time-varying interaction among the blades and the radar cross section that changes with time as well. In Figure 4, the four blades of a helicopter and the direction of the incident wave are represented at two different times assuming that the angle of elevation is zero. The parts of the blades that have a black, thick line are visible from the radar so that the received signal depends on the reflected signal from all these parts. The other parts are shadowed and do not contribute to the received signal. When the blades move, the parts of the blades that are visible change. Furthermore, the radar cross sections of the blades have changed because the angle of incidence is different [23]. Thus, an in-depth study of the radar back-scattered signal of complex targets is only possible with sophisticated simulation tools. In the next section, we take all these considerations into account to generalise the facet model developed in [13], [14] such that it can handle Assumption 1, which is reasonable enough to model helicopter blades as shown before.

III. Received signal using a facet model

We use the triangular facet model of target proposed in [13], [14] in order to take into account the varying radar cross section of the scatterers and the shadowing of different parts of the target. The triangular facet model is an intermediate model between the point-scatterer model and the electromagnetic model. Each facet is considered to be a point-scatterer, located on its phase center [13], whose radar cross section depends on the shape and the area of the triangle, the angle of incidence and the frequency. On the contrary, it should be noted that all the scatterers in the usual point-scatterer model have a constant radar cross section with respect to the angle of incidence and the frequency [3], [24]. Note that in [14] an ISAR image of a helicopter is simulated but the received signal in [14] works under Assumption 0 (stop-and-go) so the echoes from the helicopter blades are not properly modelled.

The target is composed of a set of solid objects modelled by triangular facets. Each solid object can have a different motion so the spin of the blades of a helicopter can be simulated. A block diagram of the simulator of the helicopter dynamics is shown in Figure 5. Each facet is characterised by a triangle

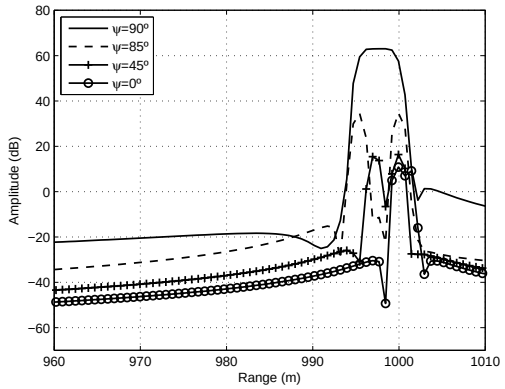

(a)

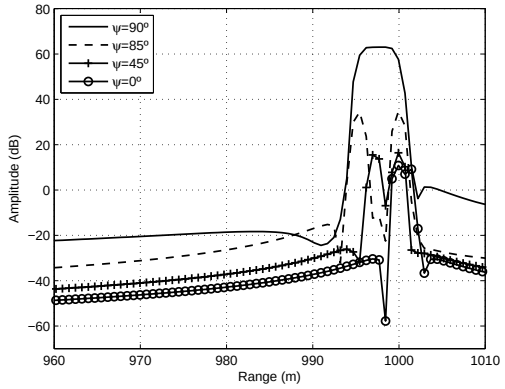

(b)

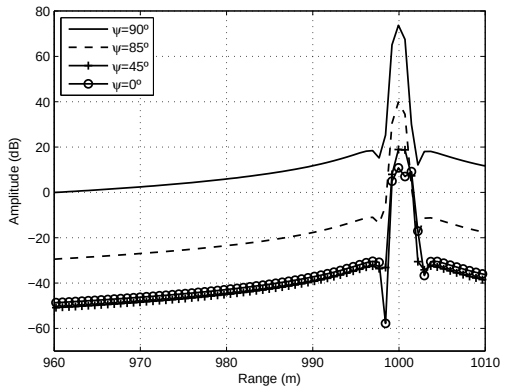

(c)

Figure 3: Range profiles of a single blade using the theoretical model in Section II for an angle of elevation α =80º: (a) Under Assumptions 2 (b) Under Assumption 1 (c) Under Assumption 0 (stop-and-go). The stop-and-go assumption is not valid for simulating the radar back-scattering from a helicopter blade using an LFMCW radar. The figures under Assumptions 1 and 2 are indistinguishable.

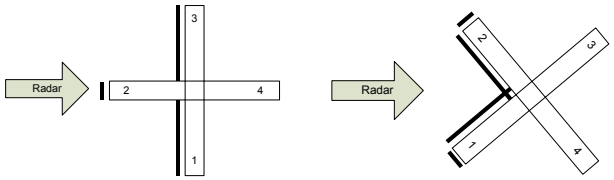

Figure 4: A thick black line is plotted to highlight the parts of the blades that reflect power at different times. It is clear that these change along time and, therefore, shadowing plays an important role.

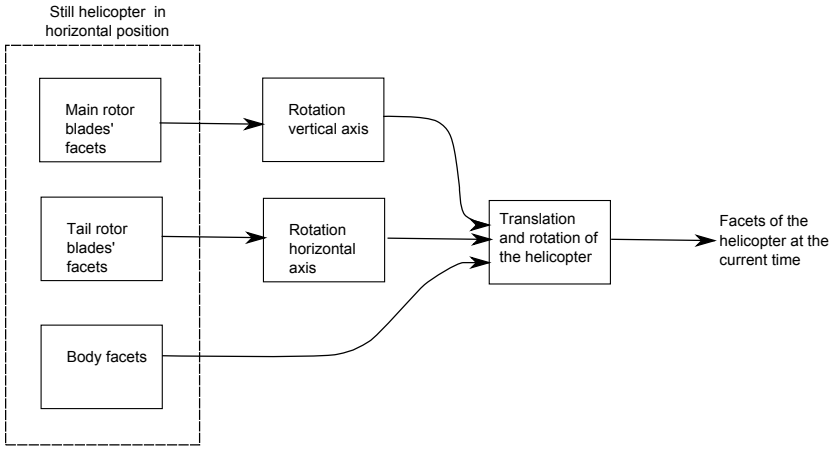

Figure 5: Block diagram of the simulator for the helicopter dynamics. The helicopter in still position is modelled by facets. At each time step, the main and tail rotor blades' facets undergo a rotation. After these rotations, all the facets are translated and rotated according to the helicopter movement. These steps are done at each time step.

and a unitary vector which is orthogonal to the triangle[3] $\hat{n}$. The direction of this vector indicates the active face of the facet. The active face is the external face of the facet in relation to the solid object that the facet belongs to. This model has been used so far for simulating ISAR images of targets and calculating accurate radar cross sections when the effect of multiple scattering is negligible. The good performance of our simulator has been checked using measured data in [13], [15] although it skips the problem of double reflections that could arise in some situations.

Then, adapting equation (12) to facets, the returned signal after the process of dechirping from a target

[3]The notation $\hat{a}$ indicates that vector $\hat{a}$ is a unitary vector

under Assumption 1 is

$$s_{facet}(t) = \sum_{i=1}^{M} \psi_i \cdot \sqrt{\sigma_i} e^{j(\phi_{20i} + \phi_{21i} t + \phi_{22i} t^2)} \tag{36}$$

where ϕ_{20i}, ϕ_{21i} and ϕ_{22i} have the same form as in equations (13), (14) and (15) but changing R_0 and v_R for R_i and v_{Ri}, R_i is the range of the facet i measured from the radar location, v_{Ri} is the radial velocity of the barycenter of the facet i, M is the number of facets of the target, σ_i is the radar cross section of the facet i and ψ_i is a function whose value is one if the facet i is visible from the radar and zero otherwise. The parameters R_i, σ_i and ψ_i are assumed to be constant during the ramp and the radar cross section of the facet i, σ_i, is calculated for the central frequency. All the details regarding the calculation of R_i, σ_i and ψ_i can be found in [13] and, therefore, are not given here.

As our simulator was originally designed under Assumption 0 [13], [14], we only needed the positions of the facets at different times and we did not calculate the velocities. Consequently, we designed our simulator so that it was able to calculate the positions of the facets at any time. Under Assumption 1, we need the radial velocities of the facets at the beginning of each ramp to calculate the radar echoes as shown in equation (36). Therefore, we define another parameter p_v that represents the percentage of time of the ramp repetition period $1/PRF$ to estimate the radial velocity. Then, the radial velocity v_{Ri} of the ith facet is estimated by

$$v_{Ri} = \frac{\overrightarrow{OO'_i}(t_0)}{\left|\overrightarrow{OO'_i}(t_0)\right|} \cdot \left(\frac{\overrightarrow{OO'_i}(t_0) - \overrightarrow{OO'_i}\left(t_0 - \frac{p_v}{PRF}\right)}{\frac{p_v}{PRF}} \right) \tag{37}$$

where t_0 represents the time the ramp starts and $\overrightarrow{OO'_i}(t)$ is the vector that goes from the radar to the barycenter of the facet i at time t.

IV. Simulation results

In this section, we use the facet model to simulate range profiles of a single blade of a helicopter and the range profiles of a complete helicopter for two elevation angles. We also compare them to the theoretical results in Section II and to the results obtained under Assumption 0 (stop-and-go). The parameter $p_v = 10^{-4}$, which is used in (37) to estimate the radial velocities of the facets. It should be noted that the duty cycle of the signal is 90% for the parameters in Table I, i.e., the sweeping time is 0.9ms and the retrace is 0.1ms.

A. Single blade

We simulate the range profiles of a blade modelled by facets with the same parameters as in Table I for the elevation angles α =0º and α =80º. The blade is modelled as a perfectly conducting plate of 5

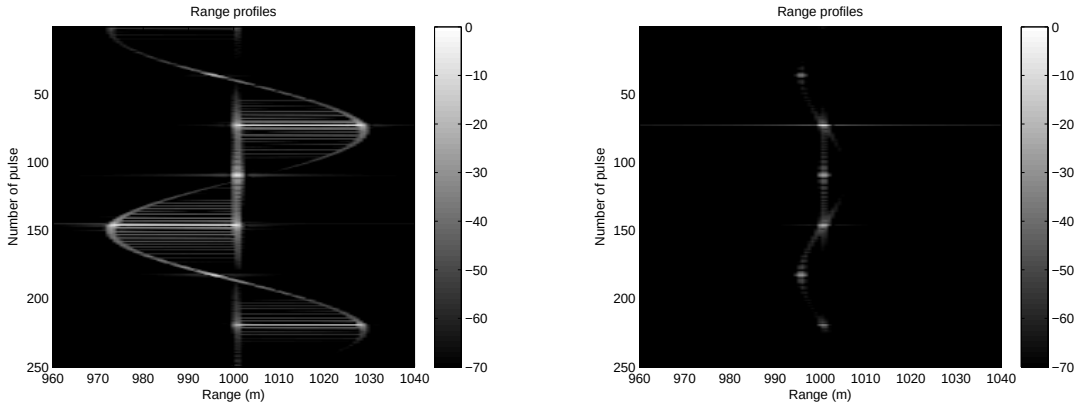

(a) (b)

Figure 6: Range profiles of a blade modelled by facets with elevation angle α =0º: (a) under Assumption 1 (b) under Assumption 0.

meters long. The range profiles normalized with respect to the maximum are shown in Figures 6 and 7.

First, let us focus on the cases that use Assumption 1. The peak on the left of the sinusoidal waveform when the elevation angle is α =0º, Figure 6(a), occurs approximately at range 970m, which is the same as the theoretical result shown in Figure 2. There are also horizontal lines of high power when the blade is orthogonal to the line of sight as can be seen in pulse number 146. However, the power of the signal changes in a different way with time because, in Figure 6(a), the radar cross section and the parts of the blade that are visible change as time goes on. The peak on the left of the sinusoidal waveform when the elevation angle is α =80º, Figure 7(a), occurs approximately at range 995m that is the same as the theoretical result shown in Figure 2. Thus, the length of the expansion of the power of the signal along the distance axis in the facet model is the same as in the theoretical model but the power of the signal in the facet model depends on the radar cross section.

The range profiles of the blade with elevation angle α =0º under the stop-and-go assumption are shown in Figure 6(b). Here, the signal goes from range 995m to range 1005m due to the fact that the blade tip actually moves from range 995m to 1005m and there is no expansion of the signal because we assume that the scatterers remain in the same position during the ramp. It is also important to notice that the signals under Assumptions 0 and 1 are 90 degrees out of phase with each other, i.e., the peaks of the sinusoidal waveform under Assumption 1, Figure 6(a), occur at the same time when the signal crosses the range 1000m (range of the rotation axis) under the stop-and-go assumption, Figure 6(b), and

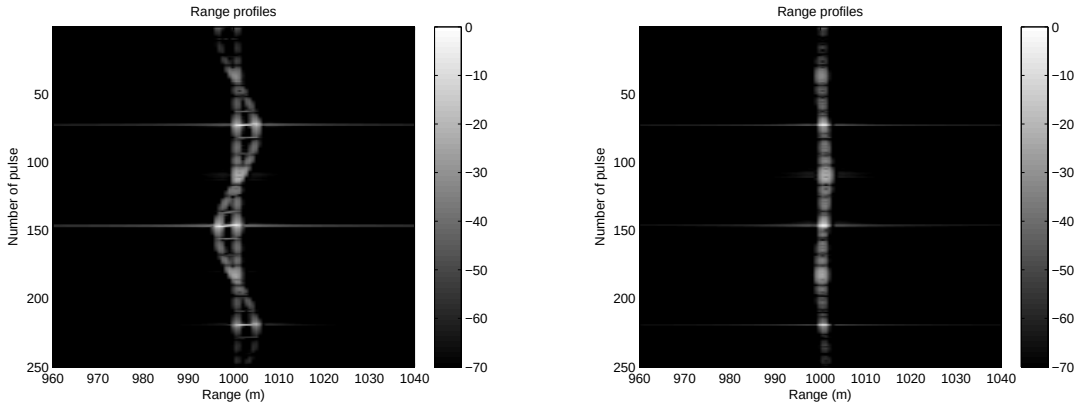

(a) (b)

Figure 7: Range profiles of a blade modelled by facets with elevation angle α =80º: (a) under Assumption 1 (b) under Assumption 0.

vice versa. The reason is that the maximum length of the expansion of the power of the signal along the distance axis in Figure 6(a) is produced when the blade is orthogonal to the line of sight but, in this position, the whole blade is approximately located at range 1000 m so it is represented as a point in Figure 6(b). Another important fact is that there are gaps at pulse numbers 36, 109, 182 and ranges 1000, 1005, 1000 in Figure 6(b), i.e., when the blade is placed along the line of sight. This fact comes from the shadowing of one end of the blade. In Figure 6(a), there are also gaps in the signal at the same pulse numbers due to the shadowing. Therefore, this implies that the stop-and-go assumption is not valid to model helicopter blades as can also be checked in Figures 7 (a) and (b) for an elevation angle α =80º. It should be noted that in Figures 7(a) and (b), the horizontal lines are due to the side lobe effects of the Hamming window used with the FFT to calculate the range profiles, see Table I.

B. Helicopter

Here, we simulate the range profiles of a helicopter with the same parameters of the previous simulations, see Table I, to study the effect of the whole helicopter on the range profiles. The model of helicopter we simulate is Bo105. This helicopter has a main rotor with four blades and a tail rotor with two blades. The lengths of the main rotor blades are 4.9 meters and the lengths of the tail rotor blades are 0.95 m. All the blades of the helicopter move with the rotation rate shown in Table I and the helicopter is hovering in both simulations. The optical images of the helicopter modelled by facets from the radar's

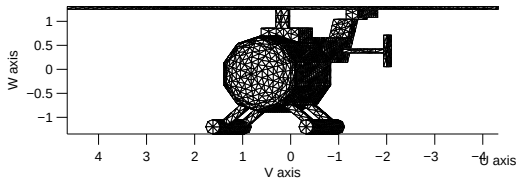

Figure 8: Optical image of the helicopter with elevation angle α =0º from the radar's point of view

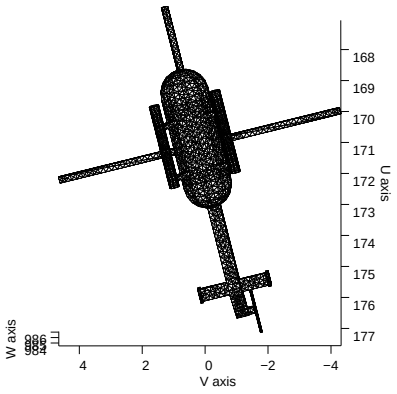

Figure 9: Optical image of the helicopter with elevation angle α =80º from the radar's point of view

point of view for both elevation angles are shown in Figures 8 and 9.

The range profiles normalised with respect to the maximum for both elevation angles are shown in Figures 10 and 11. If the angle of elevation is 0º, see Figure 10, there are long horizontal lines as happens with one blade, see Figure 6(a), but in this case the expansion occurs for closer and further ranges because there is always one blade whose elements have positive radial velocities and another blade whose elements have the same radial velocities but with negative sign. These long horizontal lines are caused by the movement of the main rotor blades. In Figure 10, the effects of the tail rotor blades can also be seen although, in this case, they are almost negligible. These effects are the short horizontal lines that are situated between two long horizontal lines, located at a range of approximately 1005-1010 meters and in approximate pulse numbers 30, 100 and 180. The frequency of appearance of these lines is

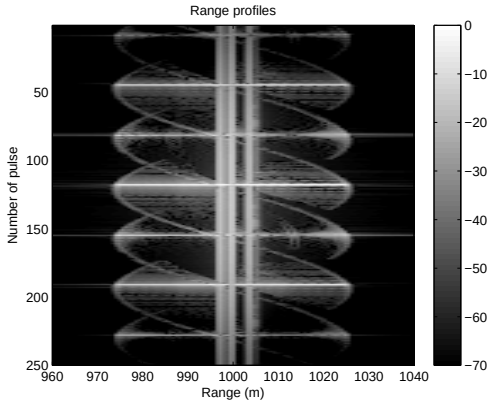

Figure 10: Range profiles of the helicopter with elevation angle α =0º under Assumption 1. The helicopter position is shown in Fig. 8 and the operating characteristics in Table I.

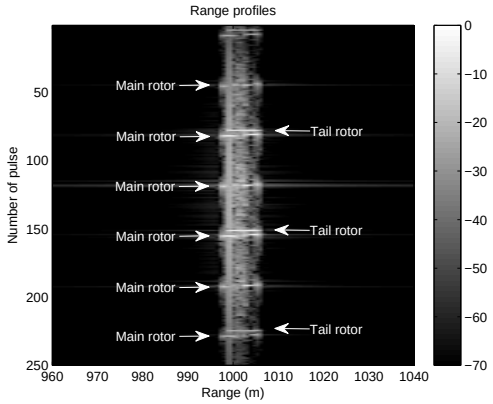

Figure 11: Range profiles of the helicopter with elevation angle α =80º under Assumption 1. The helicopter position is shown in Fig. 9 and the operating characteristics in Table I.

half the frequency of appearance of the long horizontal lines because the tail rotor has only two blades. This can be demonstrated using a simulation in which the main rotor blades are stopped as in the study performed in [14]. This expansion of the signal along the distance axis is realistic as we demonstrate in Section V with measured data.

If the angle of elevation is α =80º, see Figure 11, the long horizontal lines are not so clear as in the previous case although there is still a non-negligible expansion of the power of the signal. Furthermore, the horizontal lines of high power caused by the blades of the tail rotor have approximately the same length as the horizontal lines caused by the blades of the main rotor. This stems from the fact that the

radial velocities of the tips of the blades of the tail rotor are roughly the same as the radial velocities of the tips of the blades of the main rotor.

V. Comparison with measured data

The Microwave and Radar Group of the Technical University of Madrid has developed a high resolution LFMCW radar [19]. From the university building, we were able to illuminate a Bo105 helicopter, which is the same helicopter model that we have used in the simulations. The radar parameters that were employed to get the measurements are the same that we have used in our simulations, see Table I. The range profiles of the helicopter, in which the translational motion (range bin alignment step) has been compensated making use of the global range alignment method [25], are shown in Figure 12. We do not know the angle of elevation of the helicopter but it was approaching the university building.

There are several issues we want to highlight from Figure 12:

- We can see the long horizontal lines of high power that are provoked by the blades as we had indicated in our simulations. Similar lines have been reported in other experimental data [26].
- The lengths of the horizontal lines decrease as time goes on, i.e., with a higher number of received pulses. This could be due to the fact that the helicopter was maneuvering and, then, the plane of rotation of the blades changes and the angle of incidence is different so the length of the expansion is shorter. This effect is similar to the effect caused by varying the angle of elevation of the blades when their plane of movement is horizontal as pointed out in the appendix and simulated in Section IV, see Figures 6(a) and 7(a).
- We cannot distinguish the periodic shapes caused by movements of the tips of the blades in the range profiles, see Figure 10. This is probably due to the fact that the noise power is not low enough.
- The body of the helicopter in the measured range profiles is also properly modelled by our facet model. It appears as vertical lines of high power in both the simulations, see Figures 10 and 11, and the measurements, Figure 12.
- The expansion of the blades is around 25 meters. In the simulated range profiles for α=0º, see Figure 10, the expansion of the blades is also around 25 meters. This suggests that the elevation angle of the helicopter in the measurement with respect to the radar was relatively low as otherwise, these horizontal lines of high power would be shorter.

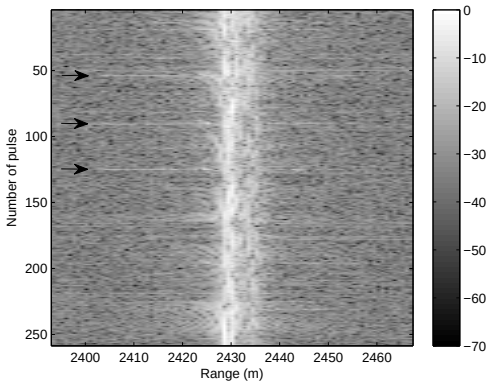

Figure 12: Range profiles of a measured capture from a helicopter. The arrows indicate where the expansion of the power of the signal along the range axis happens. This effect can be simulated by our facet model using Assumption 1.

VI. Conclusions

Our final aim is to find the main features in the radar back-scatterer signal from targets with complex motions in order to carry out classification algorithms. Therefore, as a further step to attain this goal, we have developed a simulator that calculates the radar back-scattered signal of target, which is modelled by facets and has a complex motion. The simulator also takes into account radar cross sections and shadowing. An important aspect to calculate the received signal with an LFMCW radar from a target which has parts that move with a high velocity is that the stop-and-go assumption is no longer valid.

The effects of the high speed of the blades on the range profiles are the appearance of a set a horizontal lines of high power. The lengths of these lines strongly depend on the angle of incidence of the signal with respect to the rotation plane of the blades as we have showed using a theoretical model, simulation by facets and measured data. This fact should be considered to develop classification algorithms.

Appendix

In Section II, we obtain the values of $R_0(l)$, $v_R(l)$ and $a_R(l)$ so that we are able to calculate the received signal from a blade, equation (19). It is assumed that the plane of the movement of the blade is parallel to the OUW plane but the results in Section II are general for any plane of movement of the blade if we change the definition of the $OUVW$ coordinate system. In this appendix, we redefine the $OUVW$ coordinate system to prove that the solution is general. When the general approach is followed, the $OUVW$ coordinate system depends on the plane of movement of the blades.

We assume that there is a blade of length L rotating with an angular velocity vector $\overrightarrow{\Omega}$ with respect to one of its ends O'. Now, we proceed to the calculation of the orthonormal basis $\hat{u}$, $\hat{v}$ and $\hat{w}$ that indicates the direction of the OU, OV and OW axis, respectively. There are not any constraints on the angular velocity vector $\overrightarrow{\Omega}$ so the plane of movement can be any. We also assume that the radar is located at the point O. Firstly, we define $\hat{w}$ to be parallel to the angular velocity vector $\overrightarrow{\Omega}$

$$\hat{w} = \frac{\overrightarrow{\Omega}}{\left|\overrightarrow{\Omega}\right|} \tag{38}$$

Secondly, as the point O' has to belong to the OUW plane and $\hat{v}$ has to be orthogonal to $\hat{w}$, $\hat{v}$ is orthogonal to $\overrightarrow{\Omega}$ and $\overrightarrow{OO'}$. Therefore, it is calculated via the cross product of $\overrightarrow{\Omega}$ and $\overrightarrow{OO'}$

$$\hat{v} = \frac{\overrightarrow{\Omega} \times \overrightarrow{OO'}}{\left|\overrightarrow{\Omega} \times \overrightarrow{OO'}\right|} \tag{39}$$

Finally, $\hat{u}$ is orthogonal to $\hat{v}$ and $\hat{w}$

$$\hat{u} = \hat{v} \times \hat{w} \tag{40}$$

REFERENCES

[1] M. Hagelen, A. Wahlen, and T. Brehm, "ISAR imaging of flying helicopters at millimeter-wave frequencies," in *First European Radar Conference*, Oct. 2004, pp. 265–268.

[2] X. Bai, F. Zhou, M. Xing, and Z. Bao, "High resolution ISAR imaging of targets with rotating parts," *IEEE Transactions on Aerospace and Electronic Systems*, vol. 47, no. 4, pp. 2530–2543, Oct. 2011.

[3] E. Giusti and M. Martorella, "Range Doppler and image autofocusing for FMCW inverse synthetic aperture radar," *IEEE Transactions on Aerospace and Electronic Systems*, vol. 47, no. 4, pp. 2807–2823, Oct. 2011.

[4] H. Essen, M. Hägelen, A. Wahlen, K. Schulz, K. Jäger, and M. Hebel, "ISAR imaging of helicopters using millimeter wave radars," *International Journal of Microwave and Wireless Technologies*, vol. 1, no. Special Issue 03, pp. 171–178, 2009.

[5] H. Essen, M. Hagelen, A. Wahlen, K.-H. Bers, M. Jager, and M. Hebel, "Non-cooperative classification of helicopters using millimetre wave radar and ISAR processing," in *Tyrrhenian International Workshop on Digital Communications - Enhanced Surveillance of Aircraft and Vehicles*, Sept. 2008, pp. 1–6.

[6] J. Misiurewicz, K. Kulpa, and Z. Czekala, "Analysis of recorded helicopter echo," in *Radar 97 (Conf. Publ. No. 449)*, Oct. 1997, pp. 449–453.

[7] ——, "Analysis of radar echo from a helicopter rotor hub," in *12th International Conference on Microwaves and Radar*, vol. 3, May 1998, pp. 866–870.

[8] H. Costa and M. de Matos, "Measuring time between peaks in helicopter classification using continuous wavelet transform," in *IEEE Radar Conference*, May 2008, pp. 1–6.

[9] A. Cilliers and W. Nel, "Helicopter parameter extraction using joint time-frequency and tomographic techniques," in *International Conference on Radar*, Sept. 2008, pp. 598–603.

[10] W.-D. Wirth, *Radar techniques using array antennas*, ser. Radar, sonar, navigation and avionics. The Institution of Electrical Engineers, 2001, no. 10.

[11] J. Muñoz-Ferreras, F. Pérez-Martínez, and M. Burgos-García, "Helicopter classification with a high resolution LFMCW radar," *IEEE Transactions on Aerospace and Electronic Systems*, vol. 45, no. 4, pp. 1373–1384, Oct. 2009.

[12] M. Burgos-García, M., F. Pérez-Martínez, and J. Gismero Menoyo, "Radar signature of a helicopter illuminated by a long LFM signal," *IEEE Transactions on Aerospace and Electronic Systems*, vol. 45, no. 3, pp. 1104–1110, July 2009.

[13] A. F. García-Fernández, O. A. Yeste-Ojeda, and J. Grajal, "Facet model of moving targets for ISAR imaging and radar back-scattering simulation," *IEEE Transactions on Aerospace and Electronic Systems*, vol. 46, no. 3, pp. 1455–1467, July 2010.

[14] A. F. García-Fernández, J. Grajal, and O. A. Yeste-Ojeda, "Analysis of ISAR images of a helicopter by a facet model," in *International Conference on Radar*, Sept. 2008, pp. 32–37.

[15] J. Grajal, B. Mencia-Oliva, O. A. Yeste-Ojeda, A. F. García-Fernández, and G. Rubio-Cidre, "A prototype of high resolution ISAR imaging system at millimetre-wave band," in *IEEE CIE International Conference on Radar*, vol. 1, Oct. 2011, pp. 551–554.

[16] V. Chen, C.-T. Lin, and W. Pala, "Time-varying Doppler analysis of electromagnetic backscattering from rotating object," in *IEEE Conference on Radar*, April 2006, pp. 807–812.

[17] V. Chen and W. Miceli, "Simulation of ISAR imaging of moving targets," *IEE Proceedings Radar, Sonar and Navigation*, vol. 148, no. 3, pp. 160–166, Jun. 2001.

[18] I. S. Choi, B. L. Cho, and H. T. Kim, "ISAR motion compensation using evolutionary adaptive wavelet transform," *IEE Proceedings Radar, Sonar and Navigation*, vol. 150, no. 4, pp. 229–233, 2003.

[19] A. Blanco-del Campo, A. Asensio-López, J. Gismero-Menoyo, B. Dorta-Naranjo, and J. Carretero-Moya, "Instrumental CWLFM high-range resolution radar in millimeter waveband for ISAR imaging," *IEEE Sensors Journal*, vol. 11, no. 2, pp. 418–429, Feb. 2011.

[20] W. G. Carrara, R. S. Goodman, and R. M. Majewski, *Spotlight Synthetic Aperture Radar: Signal Processing Algorithms*. Artech House, 1995.

[21] L. Weiss, "Wavelets and wideband correlation processing," *IEEE Signal Processing Magazine*, vol. 11, no. 1, pp. 13–32, Jan. 1994.

[22] G. H. Golub and C. F. Van Loan, *Matrix computations*. The Johns Hopkins University Press, 1996.

[23] D. E. Kerr, *Propagation of Short Radio Waves*. McGraw-Hill, 1951.

[24] G. Li, H. Zhang, X. Wang, and X.-G. Xia, "ISAR 2-D imaging of uniformly rotating targets via matching pursuit," *IEEE Transactions on Aerospace and Electronic Systems*, vol. 48, no. 2, pp. 1838–1846, April 2012.

[25] J. Wang and D. Kasilingam, "Global range alignment for ISAR," *IEEE Transactions on Aerospace and Electronic Systems*, vol. 39, no. 1, pp. 351–357, Jan. 2003.

[26] T. Thayaparan, S. Abrol, E. Riseborough, L. Stankovic, D. Lamothe, and G. Duff, "Analysis of radar micro-doppler signatures from experimental helicopter and human data," *IET Radar, Sonar Navigation*, vol. 1, no. 4, pp. 289–299, Aug. 2007.